

# Vibration and sound radiation of a piano soundboard

Hideo Suzuki<sup>a)</sup>

CBS Technology Center, Stamford, Connecticut 06905

(Received 24 January 1985; accepted for publication 2 September 1986)

Vibration and radiation characteristics of a piano soundboard for a 6-ft grand piano are investigated by use of modal analysis and surface-intensity methods. The mode shapes and frequencies of six resonances below 200 Hz are shown, and their relations to intensity patterns are discussed. The intensity pattern changes in a very complex manner as the frequency varies. The radiation efficiency below 80 Hz is very low. Sound is radiated fairly efficiently in the frequency range of 100 Hz–1 kHz, and very efficiently above 1.4 kHz. The results indicate that it is very important to make the input power to the soundboard as constant as possible with respect to the driving point as well as the driving frequency, in order to achieve a smooth change of sound power output from note to note.

PACS numbers: 43.75.Mn

## INTRODUCTION

The wavelengths of sounds corresponding to the lowest notes of the piano are much larger than the size of the soundboard. In this range, the sound is not radiated efficiently due to the cancellation of sounds produced by the top and bottom of the soundboard. For wavelengths corresponding to higher notes, the size of the soundboard becomes relatively large and the abovementioned cancellation gradually disappears. In this frequency region, the soundboard does not vibrate as a rigid piston, but vibrates in various modes. Then, cancellation of sound from different areas of the soundboard surface starts to take place. The cancellation depends on the speed of sound in air and the speed of the flexural wave in the soundboard. However, since the structure and the shape of the soundboard are so complex, it is very difficult to investigate the vibration and radiation characteristics theoretically. Thus studies performed in the past have been mostly experimental. Even though researchers<sup>1-4</sup> have studied the piano soundboard for many years, a good understanding of the soundboard has yet to be obtained. In the present paper, vibration and radiation characteristics of a 6-ft grand piano soundboard are investigated by use of modern measurement techniques. The modal analysis method<sup>5</sup> is applied to investigate vibration characteristics. The surface-intensity method<sup>6</sup> is used to measure sound intensity.

Vibration patterns of several lowest orders are shown and compared to the intensity patterns. The intensity patterns are also shown to much higher frequencies. Quantities obtained by integrating the intensity over the measurement surface such as the radiated power, radiation efficiency, and normalized radiation resistance are discussed. Emphasis is placed on the discussion of the radiation efficiency change as a function of frequency.

## I. MEASUREMENT

### A. Measurement setup

The block diagram of the measuring system is shown in Fig. 1. A dynamic structural analyzer (Hewlett-Packard,

5423A) was used to control the measurement system. This analyzer is designed for modal analysis of a structure in general. A bandlimited noise signal from the analyzer is fed to a shaker (MB Electronics, model EA 1500) which is connected to the soundboard by a 1.25-cm-diam brass rod with a force transducer (PCB, model 200B) at the end of the rod. The force transducer measures the excitation force  $F(\omega)$  applied to the soundboard by the shaker. This signal is used as the input to channel 1 of the analyzer. At the same time, an accelerometer (PCB, model 309A) picks up the acceleration  $\alpha(\omega)$  at a point on the soundboard. This signal is used as the input to channel 2. The analyzer calculates the acceleration-frequency response function,  $A(\omega) = \alpha(\omega)/F(\omega)$ , from the two signals and, after 16 times of averaging, stores  $A(\omega)$  on a data tape. Then, channel 2 is switched to the pressure signal  $p(\omega)$  from a microphone located at the same point as the acceleration measurement. The pressure-frequency response function,  $P(\omega) = p(\omega)/F(\omega)$ , is calculated and stored on the data tape next to  $A(\omega)$ . The same process is repeated for different locations on the soundboard, with the driving point fixed and the receiving point varied.

### B. Modal analysis

The first step of modal analysis is to assign mode numbers to the resonances which are observed as peaks of the acceleration-frequency response functions  $A(\omega)$ . Then, by choosing one representative response function from repeated measurements, the frequency and damping of each mode are calculated by use of a curve-fitting algorithm. Once the representative frequencies and dampings are given for individual resonances, the relative amplitude (including phase information) of each mode at every point is calculated again by use of the curve-fitting algorithm. This displacement vector is called a mode shape. This mode shape can be graphically animated if the coordinates of the measurement points and the display sequence are given. If necessary, the modal mass and the stiffness for each mode can also be calculated. The animated display of the mode pattern is very helpful to the understanding of vibrational characteristics.

<sup>a)</sup> Present address: Ono Sokki Co. Ltd., Tokyo, Japan.

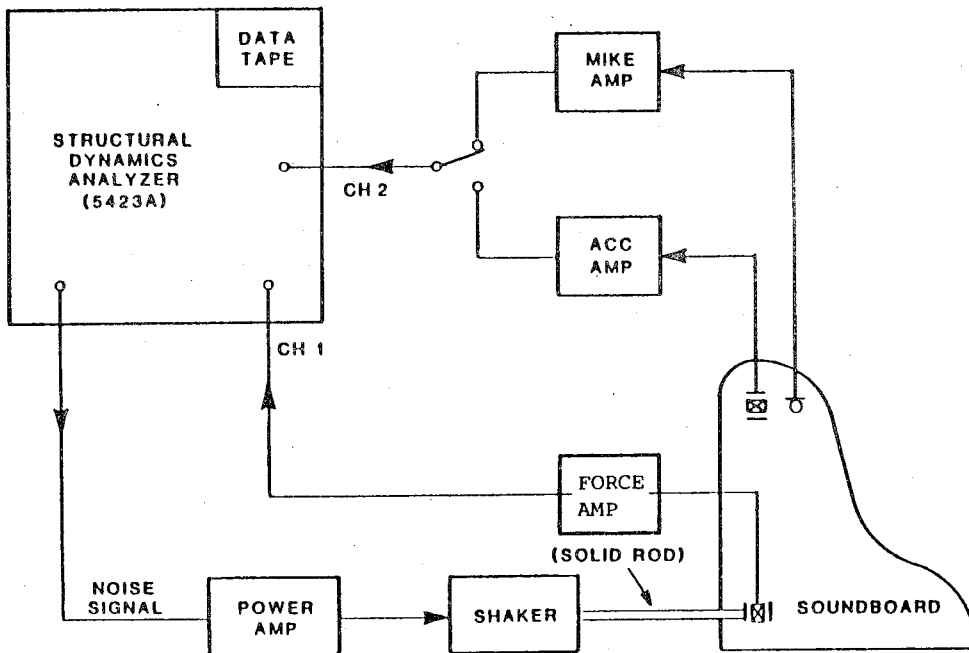


FIG. 1. Setup for the measurement of the vibration and radiation of a piano soundboard.

### C. Surface-intensity method

The time-averaged intensity perpendicular to a vibrating surface is calculated as a function of angular frequency  $\omega$  by

$$I = \text{Re}[p(\alpha/j\omega)^*]/2, \quad (1)$$

where the symbols  $\text{Re}$  and  $*$  indicate the real part and the complex conjugate of a complex number, respectively, and  $p$  and  $\alpha$  are the pressure and the normal acceleration at the measurement point, respectively, and  $j = (-1)^{1/2}$ . So that we can calculate the intensity distribution and some other intensity-related quantities, the data stored on the data tape were sent to a VAX 11/780 host computer through an IBM PC. For the animated display of the intensity pattern, the intensity distribution calculated in the VAX 11/780 was sent back to the HP-5423A structural dynamics analyzer.

When the vibration and the intensity patterns are compared, the following should be kept in mind. The intensity pattern is the intensity distribution when the soundboard is driven at a specific point and frequency. The forced vibration of the soundboard in this case contains all the modes even though only the modes near the driving frequency on the frequency axis are dominant. On the other hand, the mode shape is a pattern of a specific mode which is unrelated to the driving point and frequency.

The major drawback of the surface-intensity method is the difficulty in the phase calibration between the accelerometer and the pressure microphone. In the low-frequency range, where the radiation efficiency is small, the pressure and the velocity are almost  $90^\circ$  out-of-phase ("reactive field"), and a small error of the phase measurement results in a significant error in the intensity calculation. Therefore, the phase mismatch between the two transducers must be calibrated as accurately as possible. This was accomplished by use of the calibration device shown in Fig. 2.

The calibrator consists of an aluminum block with a small air chamber and a driver. When the driver is excited by a shaker, the sound pressure inside the chamber is  $180^\circ$  out-of-phase with the acceleration of the driver. Thus, by putting the accelerometer on the driver and facing the microphone onto the air chamber, the difference of the phase responses ( $\phi_a - \phi_p$ ) is measured, where  $\phi_a$  and  $\phi_p$  are the phase responses of the accelerometer and the microphone. The result is shown in Fig. 3. The phase difference is almost zero around 200 Hz, but it is significantly large in the low-frequency region. At 50 Hz, for example, the phase difference is about  $-10^\circ$ . This phase response was also sent to the VAX 11/780 and used for calibration when the intensity was calculated by use of Eq. (1).

### D. Test soundboard and measurement conditions

The shape and dimensions of a test soundboard of a Steinway model L (6-ft) grand piano are shown in Fig. 4. The measurement was performed on a soundboard with a rim and a brace, but without a cast-iron plate and strings. Table I shows the measurement conditions for four different measurement types. Measurement types I-IV cover the frequency range of 10 Hz-5.4 kHz. The measurement points and the areas of measurement are common for measurement types I and II and for measurement types III and IV. They are shown in Fig. 4. The shaded area in Fig. 4 is the measurement area for measurement types III and IV. The reason for using a smaller measurement area for measurement types III and IV than for measurement types I and II is to keep the number of measurement points within a reasonable range for the reduced mesh size. Approximately one-third of the whole area of the soundboard (top side only) at the lower right corner was chosen so that it included the driving point for measurement types III and IV. The two thin curves shown in the figure are the bass and treble bridges. The inter-

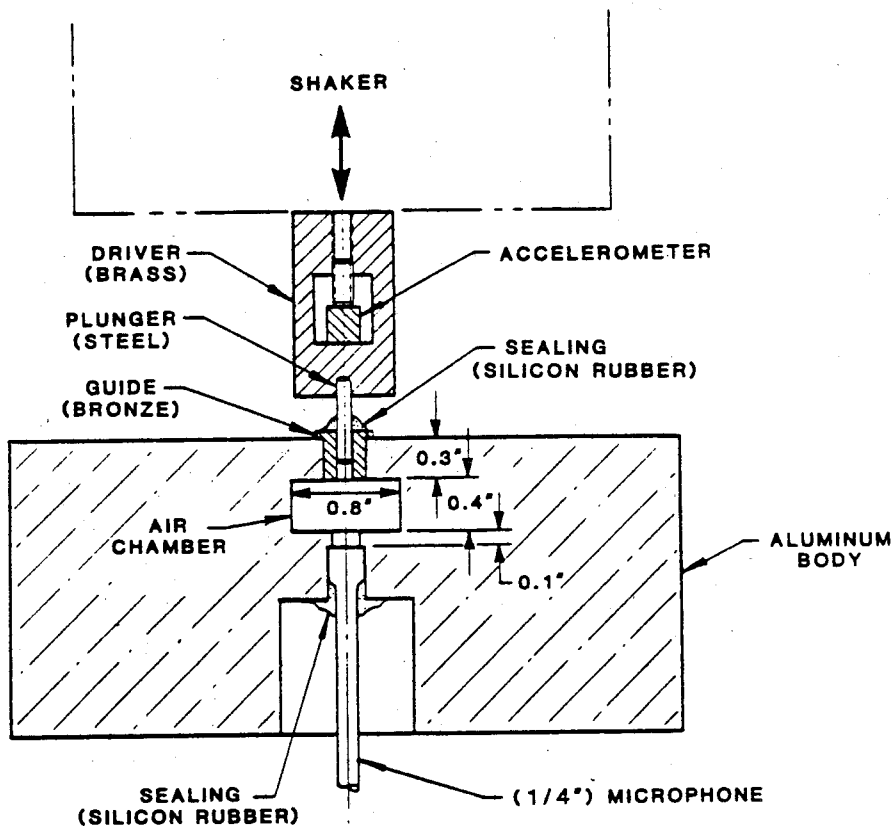


FIG. 2. Device used to calibrate the phase differences between the accelerometer and the microphone.

sections of thick lines are the measurement points for measurement types I and II, and dots on the bridge mark the driving points  $D_1$ ,  $D_2$ , and  $D_3$ . Strings for key numbers 41 ( $C_4\#$ ), 44 ( $E_5$ ), and 61 ( $A_5$ ) cross the bridges at points  $D_1$ ,  $D_2$ , and  $D_3$ , respectively.

## II. RESULTS AND DISCUSSION

### A. Vibration characteristics

The information about mode shapes and frequencies is very important in understanding the vibration characteristics of the soundboard, as well as the radiation characteristics. Figure 5 shows  $A(\omega)$  and  $P(\omega)$  at ten measurement

points in the frequency range of 10–210 Hz. In this frequency range, the two kinds of frequency response functions look very similar to each other. The numbers shown around the peaks of  $A(\omega)$  (top graph of Fig. 5) are the assigned mode numbers for the modal analysis. (The numbers shown in the bottom graph of Fig. 5 are explained in Sec. II B.) The mode shapes obtained by applying modal analysis to the acceleration responses are shown in Fig. 6.

The first vibration mode (49.7 Hz) is very simple and similar to the vibration of a trampoline. This mode will be

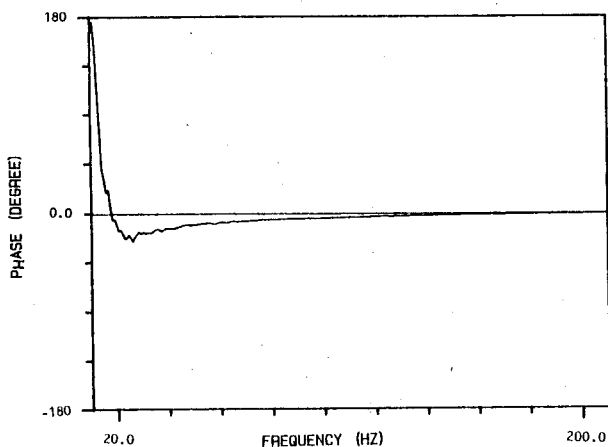


FIG. 3. Phase difference between the accelerometer and microphone responses.

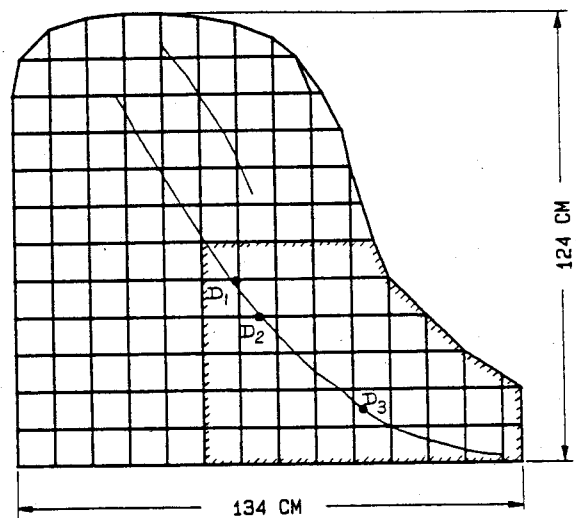


FIG. 4. Top view of the soundboard. The shaded area is the measurement area for measurement types III and IV;  $D_1$ ,  $D_2$ , and  $D_3$  are the driving points.

TABLE I. Measurement conditions.

Measurement	Frequency range	Driving point	Area of measurement	Number of measurement points	Mesh size (cm)
I	10-210 Hz	$D_1$	Fig. 4 Shaded area in Fig. 4	150	10
II	200-600 Hz	$D_2$		150	10
III	600 Hz to 2.2 kHz	$D_3$		193	5
IV	2.2-5.4 kHz	$D_3$		193	5

denoted as (0,0) mode indicating that it has no nodal lines either in the width direction or in the length direction. The 2nd mode (76.5 Hz) is the first "breakup" mode in the length direction [(0,1) mode]. The two points near the top right corner of the soundboard are on the bass bridge and show larger amplitudes than the others (this is also true for 3rd and 5th modes). The 3rd mode (85.3 Hz) is similar to the 2nd mode except that the former has a large amplitude along the edge. This mode disappears when several 25-lb bags of lead shot are put on the rim. This fact indicates that the 3rd mode is caused by the rim resonance. (The words "rim resonance" may not be correct since the rim and the soundboard are interrelated. This term, however, is used here to mean a mode which disappears when the rim is damped.) The 4th mode (116.1 Hz) is the first "breakup" mode in the width direction [(1,0) mode]. The 5th mode (135.6 Hz) is a pattern having two nodal lines in the length direction that are not parallel to the keyboard. The 6th mode (161.1 Hz) is a well-defined (1,1) mode. The first six modes have an average spacing of approximately 22 Hz between

adjacent modes. The dampings (loss factors) of the modes are very small. They are 0.064 for the first mode and approximately 0.02-0.03 for the higher modes.

The vibration characteristics shown above are expected to help us understand the radiation characteristics in the low-frequency range. Only a few distinct resonances are observed above 200 Hz, and the application of modal analysis becomes less meaningful. The Chladni method or the optical holography technique is more appropriate for the observation of the vibration patterns in the mid- to high-frequency region.

### B. Intensity pattern

The accuracy of the surface-intensity measurement depends on the accuracy of the phase calibration of the transducers and the phase difference between the velocity and the sound pressure on the surface. If the sound field is highly reactive, the accuracy of the measurement decreases. If the sound radiation is more efficient, a more accurate result is available for a given phase calibration accuracy. For the analysis of the intensity pattern in the frequency range of 10-210 Hz (measurement type I), six frequency points were chosen at which the radiation efficiency was large enough to ensure the accuracy of the intensity calculation. These points

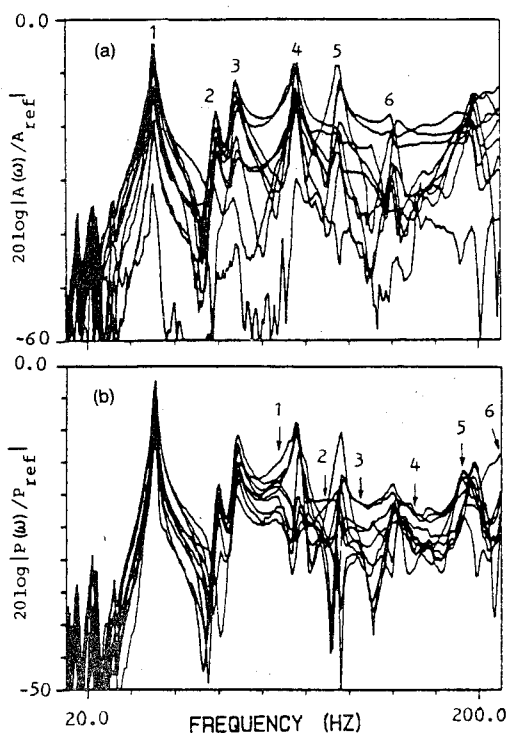


FIG. 5. Acceleration- (a) and pressure- (b) frequency response functions at ten measurement points for measurement type I.  $A_{ref} = 1/kg$ ;  $P_{ref} = 1/m^2$ .

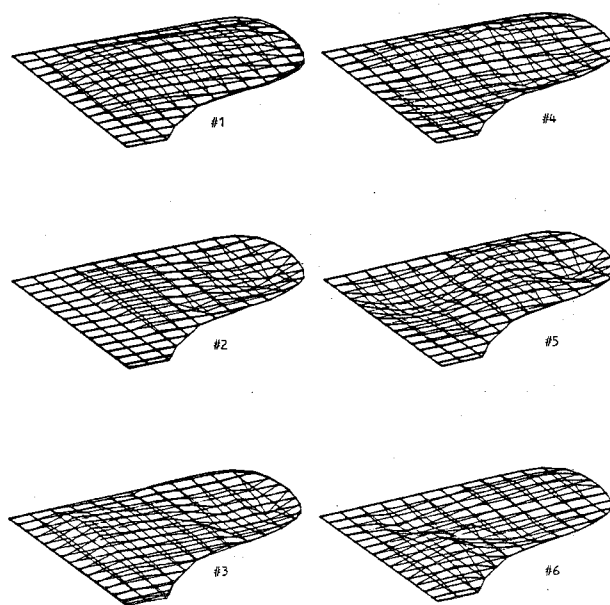


FIG. 6. Mode shapes of the first resonances. They are at 49.7 Hz (#1), 76.5 Hz (#2), 85.3 Hz (#3), 116.1 Hz (#4), 135.6 Hz (#5), and 161.1 Hz (#6).

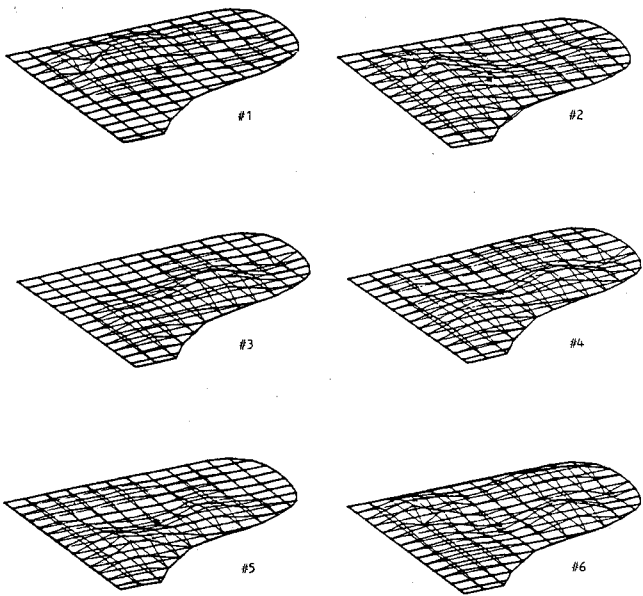


FIG. 7. Relative intensity patterns at 107 Hz (#1), 128 Hz (#2), 147 Hz (#3), 168 Hz (#4), 192 Hz (#5), and 209 Hz (#6). The driving point ( $D$ ) is shown by dots. The locations of these frequencies are shown in the bottom of Fig. 5.

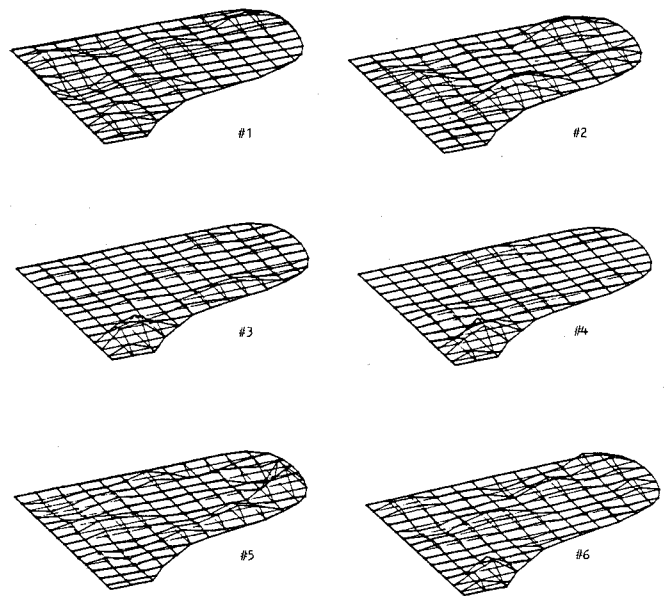


FIG. 9. Relative intensity patterns at 769 Hz (#1), 944 Hz (#2), 1.34 kHz (#3), 1.62 kHz (#4), 1.85 kHz (#5), and 1.99 kHz (#6).

are indicated by the numbered arrows in the bottom graph of Fig. 5. For measurement types II-IV, the choice of frequencies is arbitrary. Intensity patterns for measurement types I-IV are shown in Figs. 7-10. It should be noted that the intensity given by Eq. (1) is a time-averaged intensity rather than an instantaneous intensity. Also, the intensity pattern is dependent on the driving point as well as the frequency.

Below 80 or 90 Hz, the sound field is very reactive and the present measurement system does not have enough accu-

racy in this frequency region. The half wavelength of the sound in this frequency region is larger than the path length from the center of the top surface to the center of the bottom surface of the soundboard around the rim.

The intensity pattern at 107 Hz shows a large intensity region on the left side of the soundboard. This pattern is more or less like a superposition of the 3rd and 4th vibrational modes. For the intensity patterns at 128 and 147 Hz, the area of the largest intensity is at the lower middle part and right side of the soundboard, respectively. The radiation area with large intensity is restricted to a narrower region

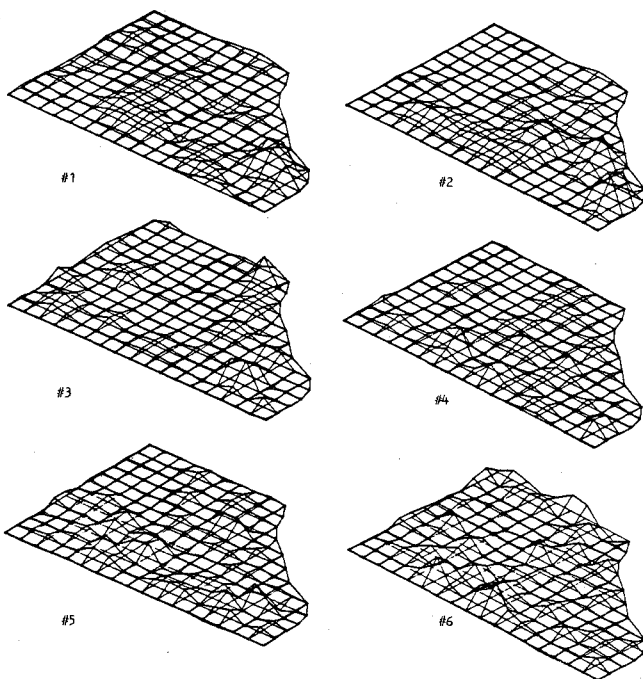


FIG. 8. Relative intensity patterns at 254 Hz (#1), 307 Hz (#2), 348 Hz (#3), 375 Hz (#4), 412 Hz (#5), and 493 Hz (#6).

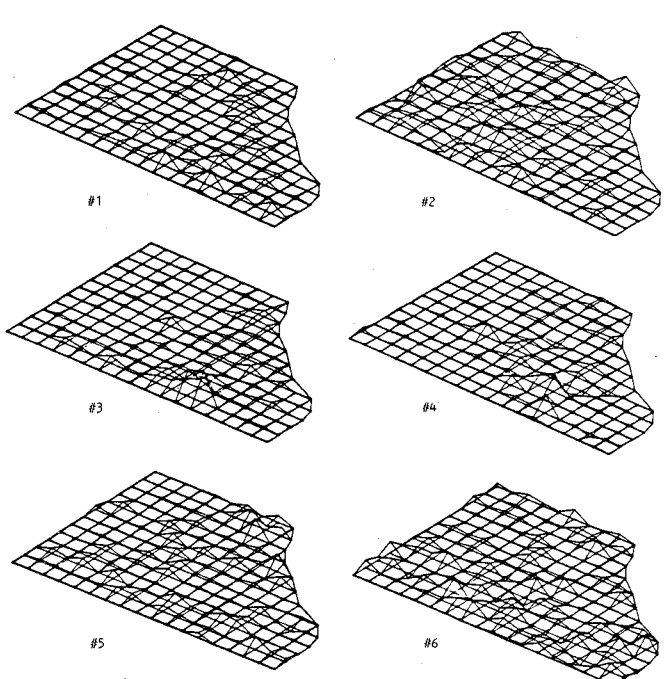


FIG. 10. Relative intensity patterns at 2.64 kHz (#1), 2.91 kHz (#2), 3.67 kHz (#3), 3.95 kHz (#4), 4.61 kHz (#5), and 4.99 kHz (#6).

than appears from the modal vibration patterns. The fact that the frequencies, at which the radiation efficiency is large, are not at or near the resonance frequencies of the board but near the midpoints among them may be explained by assuming that: (1) the cancellation of sound from different areas of the soundboard surface is the determining factor of radiation efficiency; and (2) the volume velocity of the soundboard vibration becomes large when two modes interfere strongly. The intensity patterns at higher frequencies in measurement type I have small areas with negative intensity, and the radiation efficiency is greater in this range. It is interesting that the intensity at the driving points (shown by the dots in Fig. 7) is not necessarily positive. It is expected that the sound energy absorbed into one area of the soundboard is partly consumed as a mechanical loss and partly transmitted from other areas of the soundboard.

The intensity patterns above 200 Hz (Figs. 8–10) have smaller areas with negative intensities, indicating that the “short-circuit” effect decreases as the wavelength in the air becomes close to the wavelength in the soundboard. The directional characteristics of spruce (main wood used for the soundboard) and the existence of the stiffeners and the bridges affect the sound velocities in different directions. Therefore, there is no single frequency above which the wavelength in the air is always smaller than the wavelength in the soundboard. The intensity patterns above around 3 kHz are not smooth, indicating that the unit distance of 5 cm between adjacent measurement points is not small enough above this frequency region. Also, the area of sound radiation is not limited in the area of measurement types III and IV even in the high-frequency region above 5 kHz.

Since the intensity patterns (and obviously the vibration patterns) change in a very complex manner as the frequency varies and since it is difficult to evaluate the performance of

the soundboard from this information, the vibration and the radiation characteristics (responses as a function of frequency) will be investigated as integrated quantities over the measurement area in the following sections.

### C. Radiated power

The radiated power from the measurement area  $S$  is calculated by

$$W_r = \int_S I dS. \quad (2)$$

The responses of the radiated power for the four measurement types are shown in Fig. 11 when the soundboard is driven by a force of 1 N at points  $D_1$ ,  $D_2$ , or  $D_3$ . (The driving force of 1 N was only mathematically achieved but not in the real experiment.) As mentioned before, the area of measurement  $S$  is the entire top surface for measurement types I and II, and the shaded area in Fig. 4 for measurement types III and IV.

The power radiated below 80 Hz is very low (i.e., the sound field is very reactive) except at the first resonance of the soundboard, and the accuracy of the measurement system in this region is not enough for the intensity or power measurement. In the frequency range of 100–600 Hz, the radiated power becomes large at frequencies of the soundboard resonances.

The power response, however, does not show an increasing or decreasing trend as a function of frequency. Above 600 Hz, the deviation of the radiated power is small. This is expected from the vibration characteristics since they do not have distinct peaks with large quality factors in this region. In the region 600 Hz–2.2 kHz, the power seems to increase gradually as a function of frequency and, above 2.2 kHz, it is almost constant.

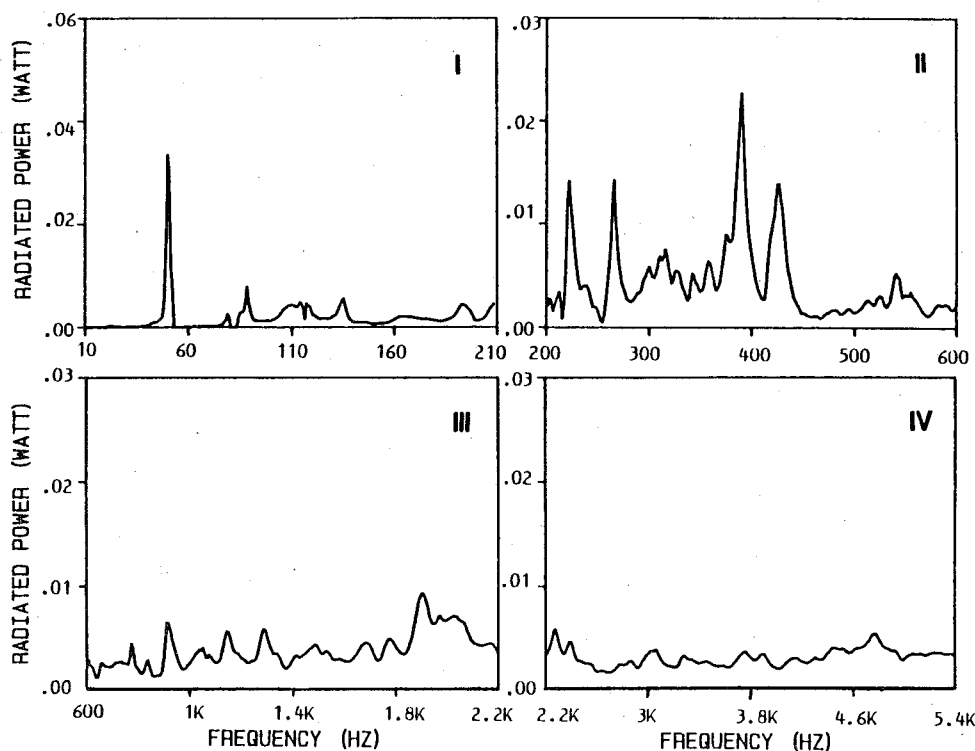


FIG. 11. Radiated power responses for measurements I–IV for a driving force of 1 N.

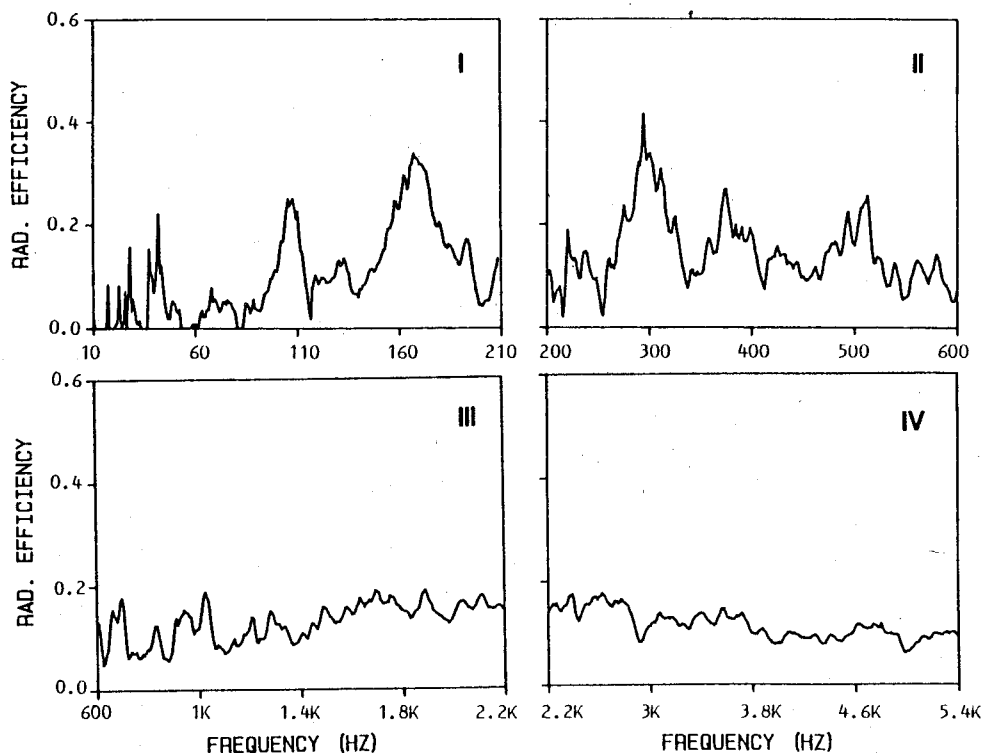


FIG. 12. Radiation efficiencies for measurement types I-IV.

#### D. Radiation efficiency

Since a constant-force excitation is different from a constant-power excitation, the power response can be viewed from a different point of view when it is normalized to the input power  $W_i$  such as

$$\eta = W_r / W_i, \quad (3)$$

where

$$W_i = \text{Re}[F_d(v_d)^*] / 2. \quad (4)$$

The input power  $W_i(\omega)$  for the unit force excitation is calculated from the measurement of the driving force  $F_d$  and the driving-point acceleration  $\alpha_d (= j\omega v_d)$ . The input power  $W_i(\omega)$  for this case will be shown in Sec. II E. The ratio of the power to the input defined by Eq. (4) will be called the radiation efficiency for convenience. It should be remembered, however, that the radiation efficiency never becomes 1.0 even if 100% of the input energy is converted to sound energy, because the measurement area covers only a part of the entire radiating surface.

Figure 12 shows the radiation efficiency for the four measurement types. In the frequency range of 100–600 Hz, the radiation efficiency fluctuates significantly as a function of frequency. It is approximately 0.15 on an average basis. The frequencies at which the radiation efficiency becomes large do not necessarily correspond to the frequencies with large radiated powers. A radiation efficiency of 0.15 in the low-frequency region seems to be very large considering the fact that the power radiated from only the top side of the soundboard is taken into account. The result of measurement type III shows that the radiation efficiency has several distinct peaks below 1 kHz. The average efficiency is approximately 0.1 in this region. Then, the response becomes

smooth and gradually increases approaching approximately 0.16 at around 1.8 kHz. Since the area of measurement for measurement types III and IV is approximately one-third that of measurement types I and II, the sound radiation is probably more efficient for measurement types III and IV than for measurement types I and II. The transition range from less efficient to efficient sound radiation is 1–1.6 kHz. This may correspond to the frequency region where the sound wavelength in the air becomes shorter than the wavelength in the soundboard. The sound wavelength in the air is inversely proportional to the frequency, whereas the wavelength in the soundboard is inversely proportional to the square root of the frequency if the complexity of the effect of the ribs and the directional characteristics of spruce are neglected. Therefore, at some frequency, the former wavelength eventually becomes shorter than the latter and, above this frequency, the radiation becomes very efficient.

#### E. Input power

The radiation efficiency ranges from 0.1–0.4 for measurement types I and II, and from 0.05–0.2 for measurement types III and IV. The radiation efficiency varies by only a factor of four for both cases. Therefore, if the frequency independence of the radiated power is a desired goal, the input power must be also frequency independent. (If the radiated power is strongly frequency dependent, the spectrum distribution may change significantly from note to note.)

Equation (4) is rewritten as

$$W_i = \text{Re}[y_d^*] \cdot |F_d|^2 / 2, \quad (5)$$

where  $y_d = v_d / F_d$  is the driving-point admittance. Equation (5) indicates that both the real part of the driving-point ad-

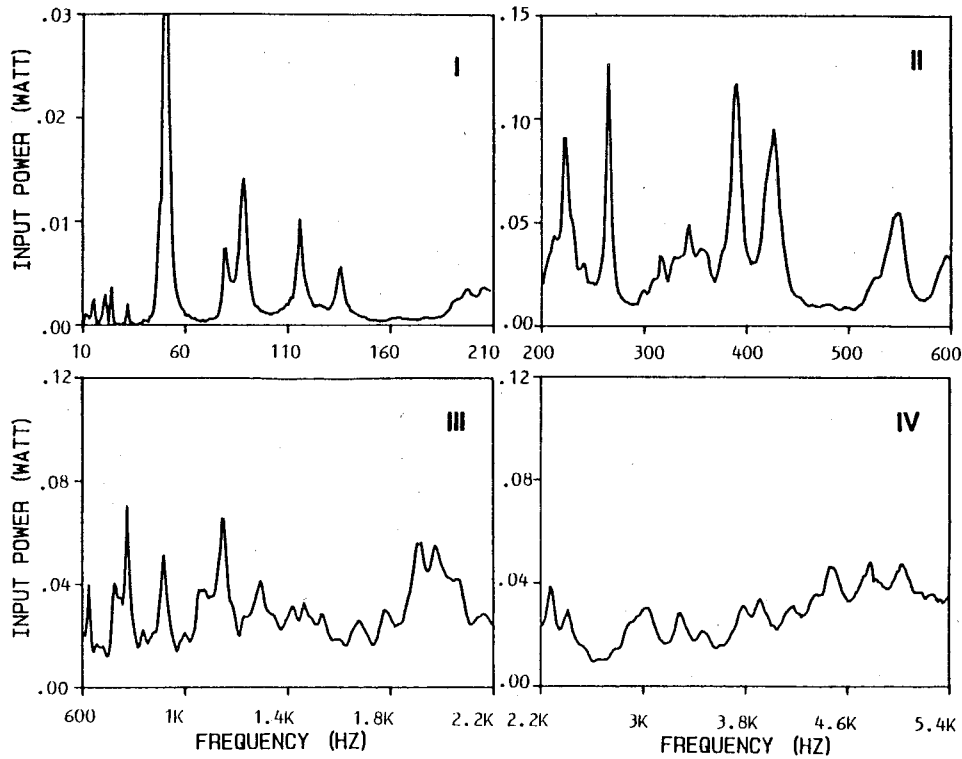


FIG. 13. Input power for measurement types I-IV for a driving force of 1 N.

mittance and the driving force must remain constant, or the product of the two must be constant in order to make the input power independent of the frequency. The input power responses for measurement types I-IV are shown in Fig. 13 for the unit force excitation (1 N).

In the low-frequency region (measurement types I and II), the input power increases significantly at the resonance

frequencies of the soundboard (except for the cases when the driving point is on or near the nodal line of a particular mode). Very sharp peaks are still observed below 1.2 kHz in measurement type III. Above this frequency, the input power shows a more gradual change. The radiated power response is smoother than the input power response below 1.2 kHz due to the "smoothing effect" of the radiation charac-

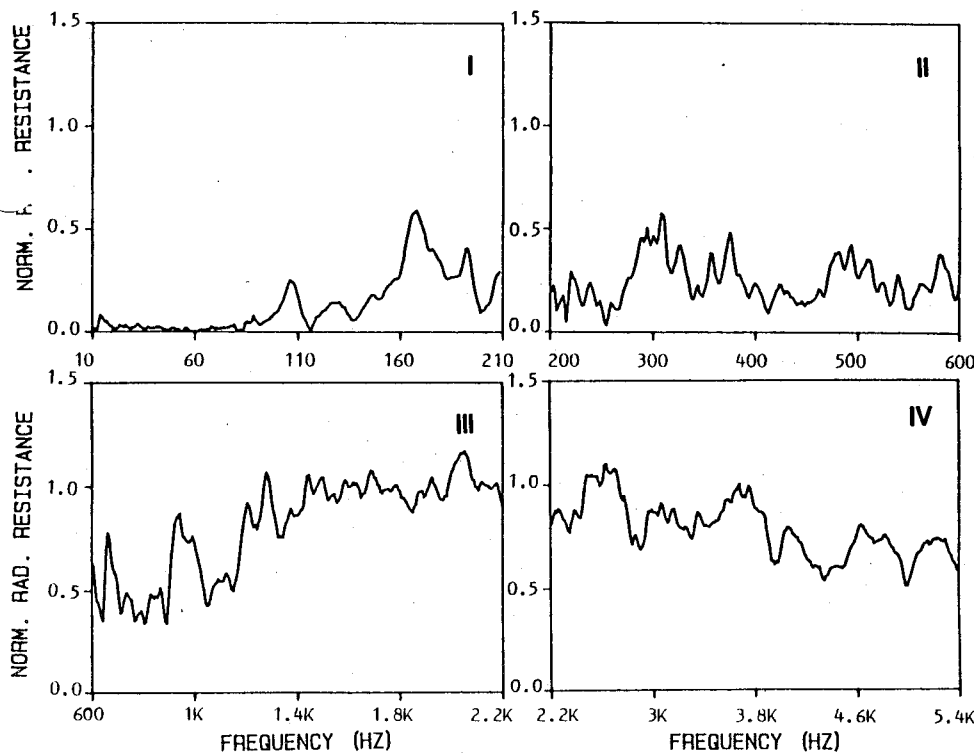


FIG. 14. Normalized radiation resistances for measurement types I-IV.

teristics; that is, radiation is less efficient at the soundboard resonances. This may be a desirable radiation characteristic for the smooth change of tone from note to note.

### F. Normalized radiation resistance

Another way of looking at the efficiency of sound radiation is the normalized radiation resistance. The normalized radiation resistance  $R$  is defined here by

$$R = W_r / \left( \rho c \int_S |v|^2 ds \right), \quad (6)$$

where  $W_r$  is the radiated power from the area of measurement,  $\rho$  is the air density,  $c$  is the sound velocity, and  $v$  ( $= \alpha / j\omega$ ) is the velocity of the soundboard at the surface element  $ds$ . The normalized radiation resistance is an index of the efficiency of radiation per unit area. Therefore, it is more meaningful to compare the radiation resistance for measurements with different measurement areas than to compare the radiation efficiencies defined by Eq. (3). The results are shown in Fig. 14. Roughly speaking, the radiation resistance is approximately 0.3 in the range of 160–600 Hz. There is a discontinuity of the radiation resistance from measurement type II and measurement type III probably due to the differences of the driving point and the measurement area. There is a sharp rise of the normalized radiation resistance in the range of 1–1.4 kHz from approximately 0.5–1.0. This transition is more clearly seen in the normalized radiation resistance than in the radiation efficiency. This indicates that the normalized radiation resistance is a useful index as a measure of the efficiency of radiation. The normalized radiation resistance seems to gradually decrease above 4 kHz. One possible reason for this is that there might be a phase measurement error of the surface pressure due to the finite distance between the microphone and the soundboard. Another possibility is that the relative phase difference between the acceleration and pressure transducers is not negligible in the high-frequency region as it is in the low-frequency region. In any case, it can be said that the radiation is efficient in the frequency range above 1.4 kHz. The critical frequency of an ideal 6-mm-thick soundboard with Young's modulus  $E = 1.4 \times 10^{10}$  N/m<sup>2</sup> (in grain direction) and density  $\rho = 400$  kg/m<sup>3</sup> is approximately 1.8 kHz. The above values of the Young's modulus and the density were obtained by measuring a plank of spruce for a soundboard. The calculated frequency is approximately 30% higher than the measured frequency at which the normalized radiation resistance is approximately equal to unity.

### III. CONCLUSION

The vibration and radiation characteristics of a soundboard (with a rim and braces) used for a 6-ft grand piano were investigated from below 100 Hz–5.4 kHz. The vibration characteristics were analyzed using the modal analysis method, and the radiation characteristics were studied by use of the surface intensity method. The soundboard used for the study shows six or seven major resonances below 210 Hz. The first (0,0) mode is at approximately 50 Hz, and its modal shape looks like a trampoline. The 2nd and 3rd modes are the first "breakup" modes in the length direction, that is, the

(0,1) mode. The difference between them is that the 3rd mode is caused by a rim resonance. The 4th mode is the (1,0) mode showing one nodal line in the width direction. The (0,2) and (1,1) modes follow in this order. The average modal density is approximately one per 22 Hz.

The time-averaged intensity patterns were shown for different frequencies between 100 Hz–5 kHz. The area with negative intensity gradually decreases as the frequency rises indicating an increase in radiation efficiency. The areas with large intensity change in a complex manner as the frequency varies.

The responses such as radiated power, input power, radiation efficiency, and normalized radiation resistance were calculated as a function of frequency. The radiation is very inefficient below 80 Hz due to the cancellation of the sounds produced by the top and bottom surfaces of the soundboard. Therefore, the discussion of the sound radiation is limited to frequencies above 80 Hz.

The input power increases significantly at the resonance frequencies below 1.2 kHz. The radiated power, however, is moderated at those frequencies due to the fact that the radiation efficiency is mostly smaller at the resonances than at other frequencies. The radiation efficiency is highly frequency dependent for frequencies below approximately 1.2 kHz, and then it levels out. The normalized radiation resistance [defined by Eq. (5)] shows a significant increase in the frequency range between 1 and 1.4 kHz, indicating that the transition from fairly efficient to very efficient radiation occurs in this region. Below 1 kHz, the normalized radiation resistance is approximately 0.3–0.5 and, above 1.4 kHz, it approaches 1.0. The fluctuation of the radiation efficiency was roughly a factor of four for all measurement cases. Therefore, a sound power output with a fairly small fluctuation can be achieved if the input power to the soundboard is independent of frequency. Since the input power is proportional to the driving-point conductance (real part of the driving-point admittance) when the soundboard is driven by a unit force, the driving-point conductance is a useful index to estimate the consistency of the radiated power. The spectrum of the force applied to the soundboard by strings may be studied experimentally or theoretically.

The present study revealed some important properties of the vibration and radiation characteristics of a piano soundboard, even though the measurement conditions such as the measurement area, number of measurement points, driving points, and frequency ranges were limited. Similar measurements should be performed on a complete piano, so that the effects of the strings, the dampers, and the plate are taken into account.

### ACKNOWLEDGMENTS

The author would like to acknowledge the useful daily discussion with his colleagues, Gordon Ebbitt and William Strong. The author would like to thank Robert Finger and Emil Torick, Directors of the CBS Technology Center, for giving the author a chance to pursue this project. He further would like to express his gratitude to KatheleneAnne Reilly at CBS Technology Center and Nanami Konami at Ono Sokki, for typing and editing the manuscript.

- <sup>1</sup>P. H. Bilhuber and C. A. Johnson, "The influence of the soundboard on piano tone quality," *J. Acoust. Soc. Am.* **11**, 311-320 (1940).
- <sup>2</sup>E. Lieber, "The influence of the soundboard on piano sound," *das Musikinstrument* **28**, 304-316 (1979).
- <sup>3</sup>K. Wogram, "Acoustical research on pianos. I. Vibrational characteristics of the soundboard," *das Musikinstrument* **30**, 694, 776, 872 (1981).
- <sup>4</sup>I. Nakamura, "The vibrational characteristics of a piano soundboard,"

*Proc. 11th ICA, Paris (1983), Vol. 4, p. 385.*

<sup>5</sup>K. D. Marshall, "Modal analysis of a violin," *J. Acoust. Soc. Am.* **77**, 695-709 (1985).

<sup>6</sup>M. C. MacGary and M. J. Crocker, "Phase shift errors in the theory and practice of surface intensity measurements," *J. Sound Vib.* **82**, 275-288 (1982).